MSc in Photonics

Universitat Politècnica de Catalunya (UPC)
Universitat Autònoma de Barcelona (UAB)
Universitat de Barcelona (UB)
Institut de Ciències Fotòniques (ICFO)

PHOTONICS**BCN**

http://www.photonicsbcn.eu

Master in Photonics

MASTER THESIS WORK

SOLITONS IN NON-LINEAR RING MICRO-RESONATORS

Salim Benadouda i Ivars

Supervised by Dr. Carles Milián Enrique, (ICFO) and Prof. Dr David Artigas Garcia (UPC, ICFO)

Presented on date 6th September 2018

Registered at

Escola Tècnica Superior d'Enginyeria de Telecomunicació de Barcelona

SOLITONS IN NON-LINEAR RING MICRO-RESONATORS

Salim Benadouda i Ivars[1]

[1]Nonlinear Optical Phenomena Group, ICFO - Institut de Ciències Fotòniques, Av. Carl Friederich Gauss, 3, 08860 Castelldefels (Barcelona), Spain

E-mail: salim.b.i95@gmail.com

Abstract. We studied with the Lugiato–Lefever spatiotemporal formalism the existence, formation and dynamics of solitons in non-linear Kerr micro-resonators. For anomalous and normal dispersion we find different types of solitons, bright and dark respectively. We have determined the region of existence and stability for both types of structures and have studied the introduction of third order dispersion which gives a velocity to the solitons and stabilises them. In the normal GVD regime, we could not find the recently proposed flat top solitons. Ideas why this is the case are discussed.

Keywords: Micro-resonator, Kerr non-linearity, soliton

1. Introduction

Optical-frequency combs have shown many applications in metrology, spectroscopy, optical clocks or sensing [1]. For years they have been generated by means of trains of ultra-short laser pulses. Lately, combs generated with micro-resonators (micro-combs) have attracted a lot of interest, in part, due to their potential on-chip integration [2]. These micro-combs are normally produced when a Kerr micro-resonator is pumped with a continuous-wave (CW) laser, leading to the generation of spectral side-bands through four wave mixing (FWM) cascade. They have been experimentally demonstrated in silica microtoroidal resonators [3, 5], in MgF_2 resonators [4] or nitride microring resonators [6]. Micro-combs are used during several hours and are expected to remain invariant during this time period. These requirements are fulfilled by dissipative solitons. The goal of this work is to gain a deeper insight into the variety of steady solutions, *i.e.*, soliton combs, in a micro-ring.

2. Modal expansion and the Lugiato-Lefever limit

A powerful way of describing the light evolution in the intracavity relies on expanding the so called modal expansion approach [7] since this method is valid for any micro-

resonator geometry. Such approach leads to the time-evolution equation for each mode amplitude. Following [8], we can express the spatio-temporal slowly varying envelope of the total field as the discrete inverse Fourier transform of these modal amplitudes, arriving to a modification of the Lugiato-Lefever equation [9], that is a continuous model, which reads:

$$-i\partial_t\psi = M(\psi, v) \equiv iv\partial_x\psi + B_2\partial_x^2\psi - iB_3\partial_x^3\psi + 2|\psi|^2\psi + (i\gamma - \delta)\psi + h, \quad (1)$$

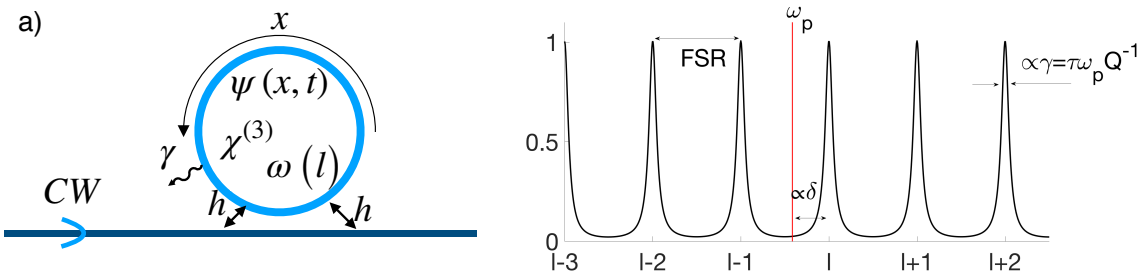

Figure 1: a) Sketch of the driven micro-ring resonator. b) Normalised transmission versus the cavity modal number. Vertical red line marks the frequency of the external driving

Equation (1) describes the propagation in time of the intracavity field dynamics $\psi(t, x)$, in the driven micro-ring sketched in figure 1 a). The time t is normalized normalised to roundtrip units, τ, x is the periodic coordinate along the micro-ring in the moving frame with the group velocity, v_{gr}, at the pump frequency, ω_p. The terms v, B_2 and B_3, account for velocity drifts from v_{gr}, the group velocity dispersion (GVD), and third order dispersion (TOD) terms of the micro-ring. They contain contributions of geometrical and material dispersion and are given by $B_q = \omega^q\tau/q!\,(2\pi R)^q$, where $\omega^{(q)} = \partial^q\omega/\partial\beta^q(\beta_p)$, here β_p is the propagation constant of the pump, R is the cavity radius. The non-linear term $|\psi|^2\psi$ in equation (1) accounts for the third order non-linear effects parametrised by the third order susceptibility $\chi^{(3)}$, of the micro-ring. Dissipation of the system is accounted for by the dimensionless photon lifetime $\gamma = \tau\omega_p Q^{-1}$, where Q is the quality factor of the micro-ring. $\delta \equiv (\omega_0 - \omega_p)\tau$ is the normalised cavity detuning between the pump frequency and the nearest cavity resonance, ω_0. With this normalised detuning, the free spectral range (FSR) becomes $\delta_{FSR} = 2\pi$. Finally, h is the coupled pump strength. In figure 1 b) we can see a sketch of the cavity resonances where l labels the different modes. Equation (1) admits localised stationary solutions, or solitons, where the Kerr non-linearity and pump counter-balance diffraction and losses. Equation (1) is invariant to the transformation $\{t, x, \psi, \gamma, \delta, h\} \to \{ta, x\sqrt{a}, \psi\sqrt{a}, \gamma/a, \delta/a, ha^{-3/2}\}$. Setting $a = \delta$ we get rid of one parameter (*i.e.* $\delta = 1$ unless stated otherwise) and so, we can take as control parameters the losses, γ, and the pump, h.

3. Numerical methods

In this section we describe the numerical tools used to find stationary solutions and to study their stability and dynamics.

3.1. Stationary Solutions

Soliton solutions are sought in the form $\partial_t \psi_s = 0$. To find them we use an iterative Newton-like (relaxation) method. The assumption at the core of the method is that the solution, ψ_s, characterised by its velocity, v_s, is well described by $\{\psi_s, v_s\} = \{\psi_g, v_g\} + \{\delta\psi, \delta v\}$, where $\{\psi_g, v_g\}$ are the guesses and $\{\delta\psi, \delta v\}$ small corrections. Thus the linearised equation for $\delta\psi$ and δv reads:

$$\mathbf{0} = \overrightarrow{M} + \hat{J}\overrightarrow{\delta\psi} + \delta v \hat{\sigma}\overrightarrow{\partial_x \psi_g}, \quad \hat{J} = \left[\begin{array}{c|c} A_+ & B_- \\ \hline B_+ & A_- \end{array}\right], \quad \hat{\sigma} = \left[\begin{array}{c|c} 0 & -1 \\ \hline 1 & 0 \end{array}\right]; \tag{2}$$

where $A_\pm \equiv B_2\partial_x^2 + 4\left|\psi_g\right|^2 - \delta \pm 2\left(\psi_g^{'2} - \psi_g^{''2}\right)$, $B_\pm \equiv \pm\gamma \pm v\partial_x \mp B_3\partial_x^3 + 4\psi_g^{'}\psi_g^{''}$ and $^{'}$ and $^{''}$ denote real and imaginary parts respectively. The vectors $\overrightarrow{M}$, $\overrightarrow{\delta\psi}$ and $\overrightarrow{\partial_x\psi}$ are built as $\overrightarrow{S} = \left[S^{'}\ S^{''}\right]^{\intercal}$, where $^{\intercal}$ stands for the transpose and S stands for M, $\delta\psi$ and $\partial_x\psi$. Lengths of $\overrightarrow{S}$ are $2N_x$, being N_x the number of sample points in x. We implement the derivatives as five point stencil finite different matrices [10]. Equation (2) is a system of $2N_x$ equations, while we have $2N_x + 1$ unknowns if $v \neq 0$. When the system is underdetermined (*i.e.*, when $v \neq 0$), we reduce in one the number of unknowns by assuming that either $\delta\psi^{'}$ or $\delta\psi^{''}$ are zero at one point, $x = a$. Hence $\delta v = -\left(\hat{J}^{-1}\overrightarrow{M}\right)_{x=a} / \left(\hat{J}^{-1}\hat{\sigma}\overrightarrow{\partial_x\psi_g}\right)_{x=a}$ and $\overrightarrow{\delta\psi} = \hat{J}^{-1}\left(-\overrightarrow{M} - \delta v\hat{\sigma}\overrightarrow{\partial_x\psi_g}\right)$. The input guess is updated with the obtained corrections, and the process is repeated until $\overrightarrow{\delta\psi}$ and δv are zero at machine precision.

3.2. Stability Analysis

In order to study the stability of our numerical solutions, we analyse the associated growth of small perturbations $\epsilon = a\,(x,y)\,e^{\lambda t} + b^*\,(x,y)\,e^{\lambda^* t}$, $|\epsilon| \ll |\psi_s|$. By substituting the perturbed field $\psi_s + \epsilon$ into equation (1) and linearising in ϵ we obtain the eigenvalue problem:

$$\lambda \left[\begin{array}{c} a \\ b \end{array}\right] = \hat{G}\left[\begin{array}{c} a \\ b \end{array}\right], \quad \hat{G} \equiv \left[\begin{array}{cc} A & B \\ B^* & A^* \end{array}\right]; \tag{3}$$

where $A \equiv -\gamma - v_s\partial_x - B_3\partial_x^3 + i\left(B_3\partial_x^2 + 4\left|\psi_s\right|^2 - \delta\right)$ and $B \equiv i2\psi_s^2$. For stable solutions ψ_s, we will find an exponential decay of all the perturbations, *i.e.* $\mathrm{Re}\{\lambda\} \leqslant 0$, $\forall\lambda$ in the spectrum of $\hat{G}$, therefore they propagate with strictly stationary profiles [*cf.* figure 3 b) and figure 6 b) for $t > 50$]. For unstable solutions, there will be typically a pair of Hopf eigenvalues with $\mathrm{Re}\{\lambda\} > 0$ associated to growing internal modes of the soliton (see discussion in section 5). Although linear stability analysis accurately predicts when

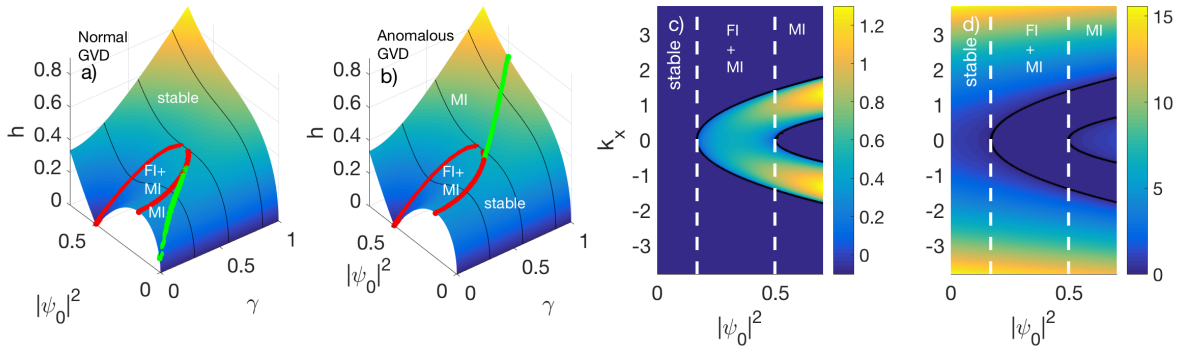

Figure 2: 1D HSSs and their stability for $\delta = 1$, $B_3 = 0$ and . a) For normal dispersion $B_3 = -1$ and b) for anomalous dispersion $B_3 = 1$. c) Gain spectrum $\mathrm{Re}\{\lambda\}$ of HSSs and d) $\mathrm{Im}\{\lambda\}$ for $\gamma = 0.1$.

solutions are unstable, it cannot provide information about the dynamics far from the unperturbed state. That information is obtained via numerical propagation simulations, described below.

3.3. Time evolution

Propagations are carried out by the Split-Step pseudospectral method (see *e.g.* [11]) with a small variation to take pump into account. We rewrite equation (1) as $\partial_t \psi = \left(\hat{D} + i2\left|\psi\right|^2 + i\frac{h}{\psi}\right)\psi$, where $\hat{D} \equiv i\left(B_3\partial_x^2 - iB_3\partial_x^3 + i\gamma - \delta\right)$ is the linear part. The introduction of the pump term in this way is in general potentially problematic as the term h/ψ becomes singular for $|\psi| \to 0$. However this is not problematic for us since our study is focused around stationary solutions that we know that have non null modulus. This is due to the external pump itself that excites the field inside the cavity and forces it to be different from zero. Comparisons with the slower Runge-Kutta methods confirm this statement.

4. The Homogeneous Steady State and its stability

Solitons in driven micro-cavities are embedded in a background field set by the external pump [*cf.* figure 4 c) and figure 6 c)]. The stability of this background is therefore crucial for solitons and is analysed in first place. The amplitude of the background or Homogeneous Steady State (HSS) can be found from the relation $h^2 = 4\left|\psi\right|^6 - 4\delta\left|\psi\right|^4 + (\gamma^2 + \delta^2)\left|\psi\right|^2$ which is straightforward from equation (1). This bicubic polynomial has three roots $|\psi|^2$, if $\gamma < \delta/\sqrt{3}$, exhibiting the so called bistable behaviour. When performing the linear stability analysis with a perturbation $\epsilon = ae^{i\delta kx+\lambda t} + b^* e^{-i\delta kx+\lambda^* t}$ as described in (section 3.2) we obtain the stability charts shown in figure 2 a) for normal GVD and figure 2 b) for anomalous GVD. In both cases, we can see three different regions: stability, flat instability (FI) together with modulational instability

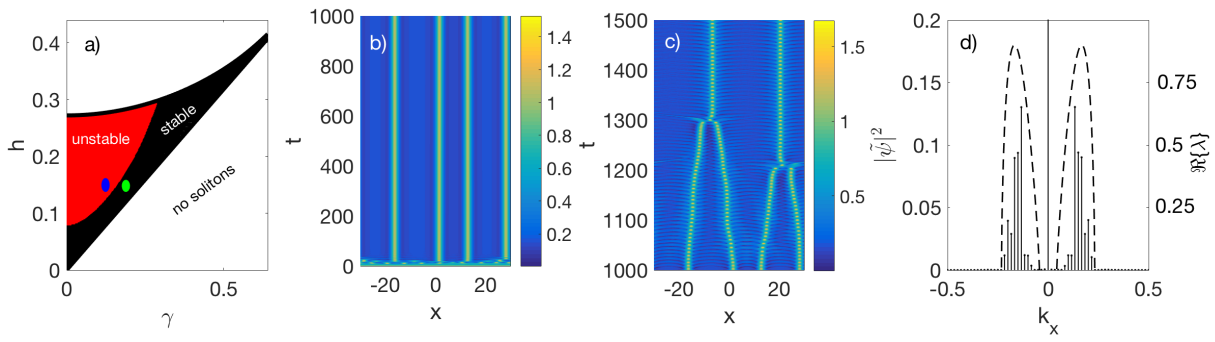

Figure 3: a) Stability and existence chart of the soliton family ψ_-. b) Stable soliton generation via MI for $\gamma = 0.2$ and $h = 0.15$. c) Time propagation continuation of b) for the breathing solitons with $\gamma = 0.13$. d) Spectrum of b) at $t = 8$ (left axis) and MI gain (right axis).

(MI), and MI alone. For the FI, the perturbations have an exponential growth for $\delta k = 0$ (*i.e.* for flat perturbations), so the HSS itself will contribute to the growth of the perturbations and therefore these solutions are intrinsically unstable. MI is an effect resulting from highly efficient FWM where two pump photons are transformed into two sideband photons through the Kerr nonlinearity [1], and therefore perturbations grow at $\delta k \neq 0$ values (*i.e.* for modulated perturbations). For normal dispersion [*cf.* figure 2 a)] MI appears in the lower branch for a finite range of γ (from $\gamma = 0$ to $\gamma \approx 0.477$) while for the anomalous case [*cf.* figure 2 b)] it appears for $\gamma \in \mathbb{R}_{\geq 0}$. In figure 2 c) and d) we see an example of the gain spectrum, $\mathrm{Re}\{\lambda\}$ and $\mathrm{Im}\{\lambda\}$ versus power of the HSS for anomalous dispersion, $\gamma = 0.1$ and $B_3 = 0$. The two dashed lines delimit the bistable region, where FI and MI coexist. The black curves in figure 2 c) and figure 2 d) mark the instability thresholds $\mathrm{Re}\{\lambda\} = 0$. We note that the eigenvalues rising the instabilities have $\mathrm{Im}\{\lambda\} = 0$, meaning that the growing perturbations oscillate at the pump frequency, together with the HSS.

5. Anomalous GVD: Bright Solitons

For $B_3 = 1$, $\gamma = 0$ and $B_3 = 0$, equation (1) admits a pair of soliton solutions $\psi_\pm$ [12]. Below, we focus on the ψ_- family since ψ_+ is unstable for $\gamma \neq 0$. Taking ψ_- as initial guess, we built the existence and stability chart shown in figure 3 a) by means of the simulations outlined in section 3.1, hence reproducing the results in [12]. In this figure we can see that, typically, instability regime is achieved by decreasing losses, γ or increasing pump, h. For the region where MI coexist with stable HSSs [*cf.* figure 2 b)], HSSs with MI can be used to excite stable solitons nested in the stable lower HSSs, as shown in figure 3 b) for $\gamma = 0.2$ and $h = 0.15$, for $t < 10$ (see below). This parameters are just above the Hopf threshold in figure 3 a), marked with a green dot. Therefore, if γ is decreased to $\gamma = 0.13$ (blue dot in figure 3 a)) the solitons become unstable and exhibit breathing behaviour as showed in figure 3 c). To illustrate the role of MI in the

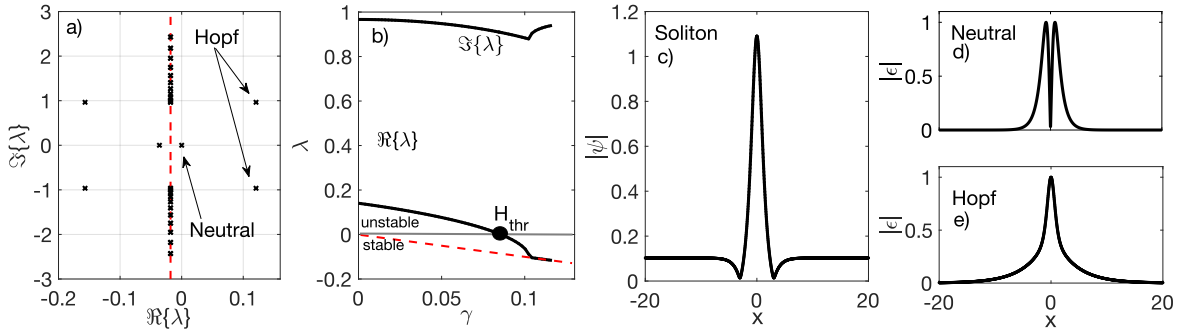

Figure 4: a) Spectrum of in the complex plane for $h = 1$ and $\gamma = 0.018$. The red dashed line indicates $\mathrm{Re}\{\lambda\} = -\gamma$ b) Maximum growth rate, $\mathrm{Re}\{\lambda\}$, and $\mathrm{Im}\{\lambda\}$ as a function of γ for $h = 1$. c) Soliton profile. d) Normalised Neutral mode (top) and hopf (bottom) modes.

soliton generation, we ploted in figure 3 d) the spectrum of the first stages ($t = 8$) of the propagation shown in figure 3 b). We have displayed the computed side lobes of the gain spectrum as the black dashed curve (see right axis) and the intracavity field spectrum as vertical bars, corresponding to the comb lines (see left axis). The transition from stable to unstable solitons is associated to a Hopf bifurcation in the spectrum of $\hat{G}$ [*cf.* equation (3)]. In figure 4 a) we show the spectrum of $\hat{G}$ for $\gamma = 0.018$ and $h = 0.1$, corresponding to an unstable soliton. Instability is therefore characterised by the pair of complex eigenvalues with $\mathrm{Re}\{\lambda\} > 0$ ad $\mathrm{Im}\{\lambda\} \neq 0$. Having a non-zero imaginary part makes the instability grow at different frequencies than the pump. This results in a breathing of the soliton amplitude and width in time, for unstable solitons. In figure 4 a) we also see an eigevalue at $(0, 0)$. Equation (3) always has this zero eigenvalue associated to the eigenfunction $\overrightarrow{\partial_x \psi}$ that corresponds to the neutral mode. In figure 4 b) we trace the Hopf eigenvalues versus γ and see how they detach from $\mathrm{Re}\{\lambda\} = -\gamma$ (dashed line) when γ is reduced. In figure 4 c), d) and e) we have represented the soliton, the neutral and the Hopf modes respectively. Because the neutral mode is proportional to the space derivative of the soliton, $\epsilon_N \propto \partial_x \psi$, such mode is associated to small spatial translations. From the Hopf modes we see that these modes are localised in the soliton but their tails exhibit a slower decay to the HSS than the soliton. That is why in figure 3 c), when the solitons become unstable they start to interact with each other repulsively or attractively. This interaction induces them a small velocity in the frame defined by x. Since we know that solitons, no matter whether they are stable or unstable, have zero velocity, we can conclude that the normal mode is also excited and is responsible for the small drift they suffer. Once the number of unstable solitons is reduced, ($t > 1300$ in figure 3 c)), they don't see each other and recover the zero drift propagation.

From equation (1) we can extract some useful information about the solitons of the system from the power integral $P \equiv \int_0^L |\psi|^2 x$ and the mean momentum $\langle k \rangle \equiv \int_0^L \tilde{\psi} k \tilde{\psi} dk / P$ whose evolution, according to equation (1), are given by

$$\partial_t P = -2\gamma P + 2h \int_0^L \mathrm{Im}\{\psi\} dx \quad \text{and} \quad \partial_t \langle k \rangle = -\frac{2h \langle k \rangle}{P} \int_0^L \mathrm{Im}\{\psi\} dx. \tag{4}$$

Stable solitons have, by definition of stationary solution, $\partial_t P = 0$ and $\partial_t \langle k \rangle = 0$. From the first condition we observe that since the losses, γ, power, P and pump , h are positive quantities, the imaginary part of the soliton $\mathrm{Im}\{\psi\}$ integrated over the micro-resonator has to be always positive for $\gamma > 0$, or zero for the undamped case, $\gamma = 0$. We also corroborate the intuitive thought that if the system has losses we need an external pump in order to get solitons. The evolution of $\langle k \rangle$ can be simplified (by combining both expressions in equation (4)) for stationary solutions as $\partial_t \langle k \rangle = -2\gamma \langle k \rangle$. We can extract two important facts from this equation. First, for a lossy medium the mean momentum has to be zero, *i.e.* the soliton is locked to the external pump. For realistic micro-resonators this will always be like that, since we can not achieve perfect $\gamma = 0$. Second, for fields not locked to the pump, the system will end up locking them since $\langle k \rangle = 0$ is a sink point.

When considering a micro-resonator whit TOD, $B_3 \neq 0$ [*i.e.*, if we move the pump frequency close to the zero GVD point] we can find radiating bright solitons. The space profile and spectrum of these solitons are no longer symmetric and so they have a constant velocity. This is because emission of the radiating tail produces spectral recoil [13] in order to fulfil $\partial_t \langle k \rangle = 0$ and therefore the carrier frequency of the soliton is shifted from the pump. We can see both the space profile of stable radiating soliton in figure 5 a) and its associated spectrum in figure 5 b). From the latter, we see the new peak that appears due to the radiation of the soliton at $k_x \approx 0.43$ and how the soliton spectrum around the pump gets modified and suffers the recoil to the left from $k_x = 0$ to $k_x = -0.05$. When taking B_3 as the control parameter, we can see how the introduction of the TOD induces a velocity of the soliton due to the $k_x = -0.05$. This effect is shown in figure 5 c). The introduction of TOD has also proved to stabilise bright solitons [15, 16, 17]. This effect is shown in figure 5 d) where we can see the real part of the Hopf eigenvalues as a function of the TOD coefficient. We see how the growth rate $\mathrm{Re}\{\lambda\}$ effectively decreases for larger B_3. We have seen that high losses, γ, stabilise the soliton [*cf.* figure 3 a)]. The radiating tail is extracting energy from the soliton, just as the losses, γ, so for unstable solitons with no TOD, the introduction of B_3 induces an extra energy loss that gets to stabilise them. In the simulations we have increased B_3 to 0.5, but [15, 14] show that bright solitons and dark solitons can exist for $B_3 \to \mathrm{inf}$.

6. Normal GVD: Dark Solitons and platicons

Dark solitons are a different type of structures that can be found in micro-resonators with normal GVD. These solitons are nested in the stable upper HSS and form a localised dip in the power of the field. Dark solitons are expected to exist when the higher and lower

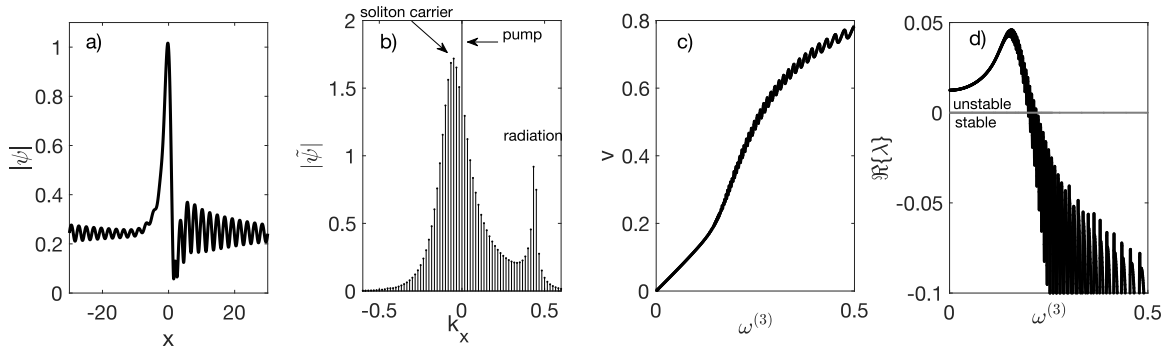

Figure 5: a) Space profile of stable radiating bright soliton for $B_3 = 1$, $\gamma = 0.2388$ and $h = 0.2388$. b) Spectrum of a). c) Velocity of the soliton as a function of B_3 and d) growth rate Re$\{\lambda\}$ as a function of B_3.

HSSs are stable. These structures have shown to exist as a snaking connection branch between the two stable HSSs [18]. We were able to excite a dark soliton by going to the region of small γ and h and propagating an upper HSS state with a broad dip. From this soliton we built the stability and existence chart of its family just as for the bright soliton ψ_-. We see in figure 6 a) that the region of existence of these dark solitons gets drastically reduced compared to one for the bright solitons. In figure 6b) we show the time propagation of a stable dark soliton and the continuation of the propagation for a lower γ in order to destabilise it (analogously to figure 3 c)). We see how the breathing behaviour also appears for dark solitons. We have studied the fundamental dark solitons, with one oscillation in its dip since it is the family with the largest existence region [18]. In figure 6 c) we plot the fundamental soliton (red), and two higher order ones (black, yellow). Dashed horizontal lines mark the higher and lower stable HSSs. We see how these families are nested in the higher branch, and the dips tend to the lower HSS.

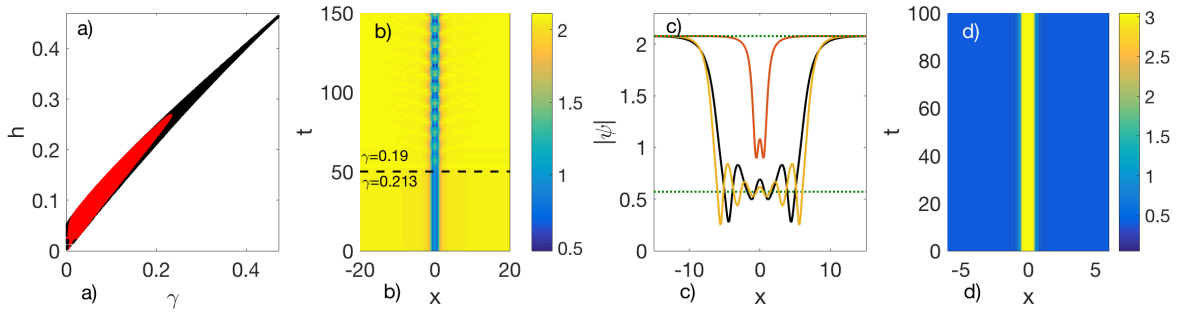

Figure 6: a) Stability and existence chart of the fundamental dark soliton. b) Time propagations of a stable dark soliton for $\gamma = 0.213$ and $h = 0.23$ for $t = [0, 50)$ and for an unstable one for $\gamma = 0.19$ for $t = [50, 150]$. c) Different families of dark solitons for stable parameters of b) with 1 (red), 3 (black) and 5 (yellow) oscillations. Dashed lines correspond to the two stable HSS. d) Time propagation of an hypotetical platicon for $\gamma = 1$, $h = 4$ and $\delta = 10$.

Another structures that have been reported are flat-top pulses called platicons [19, 20]. In order to understand this structures we have to take into account the switching waves (SWs). This waves are travelling states that connect the stable higher and lower HSSs. Because of periodicity of the micro-resonator, this waves have to go in pairs. The SW have a monotonically slope from the higher state while they end in the lower state in an oscillatory way [18]. These states can help us to understand dark solitons. Dark solitons are the connection of two SWs that get coupled with each other by their oscillating tails in the lower HSS, as clearly seen from figure 6 c) [18]. Platicons are conceived as 'complementary' to dark solitons, *i.e.* 2 SWs are linked by the higher HHS. However, some authors recently pointed at that such bonding of SWs can be difficult, if not impossible, because the SWs top state ha no oscillations. We have studied these platicons in propagation, as shown in figure 6 d). Sufficiently long simulations always revealed repulsion or collapse of the SWs. In addition, the stationary solution solver (from Section 3.1) always diverge. Therefore, a conclusion of our study is that such states seem not to exist, at least in the context of equation (1) with $B_3 = 0$.

7. Conclusions

In this work we have studied the basic properties of the one dimensional micro-ring soliton combs in the normal and anomalous GVD regimes. We have analysed their existence and stability features, in particular we found that instabilities in this system are triggered by the growth of Hopf instability, associated to the growth of soliton internal modes. We have also analysed the stability of the background flat states of the cavity which is crucial for solitons. In addition we studied the effect of the radiation induced by TOD to bright solitons and how this stabilises them. Finally we attempted to investigate the recently proposed bright solitons in the normal GVD, the so called platicons. Even if this structures might seem to exist in the numerical propagation simulations, exact computation of this states always diverged.

8. Acknowledgements

I would like to thank the whole Nonlinear Optical Phenomena Group at ICFO for giving me support and guidance, specially to Carles Milián for all his thoughtful advice.

References

[1] Y. Chembo, Kerr optical frequency combs: theory, applications and perspectives, *Nanophotonics*
[2] T Kippenberg, A. Gaeta, M. Lipson and M. Gorodetsky, Dissipative Kerr solitons in optical microresonators, *Sciencie*
[3] T. Kippenberg, R. Holzwarth and S. Diddams, Microresonator-Based Optical Frequency Combs, *Science*
[4] T. Herr, V. Brasch, J. Jost, C. Wang, N. Kondratiev, M. Gorodetsky and T. Kippenberg, Temporal solitons in optical microresonators, *Nature Photonics*

[5] P. Del'Haye, T. Herr, E. Gavartin, M. Gorodetsky, R. Holzwarth and T. Kippenberg, Octave Spanning Tunable Frequency Comb from a Microresonator *Physical Review Letters*

[6] Y. Okawachi, K. Saha, J. Levy, Y. Wen, M. Lipson, and A. Gaeta, Octave-spanning frequency comb generation in a silicon nitride chip, *Optics Letters*

[7] Y. Chembo and N. Yu, Modal expansion approach to optical-frequency-comb generation with monolithic whispering-gallery-mode resonators, *Physical Review A*

[8] Y. Chembo and C. Menyuk, Spatio-temporal Lugiato-Lefever formalism for Kerr-comb generation in whispering-gallery-mode resonators, *Physical Review A*

[9] L. Lugiatio and R. Lefever, Spatial Dissipative Structures in Passive Optical Systems *Physical Review Letters*

[10] M. Abramowitz and I.Stegun 1970, *Handbook of Mathematical Functions with Formulas, Graphs, and Mathematical Tables* (Dover: NBS)

[11] G. Agrawal 2006, *Nonlinear Fiber Optics* (New York: Academic Press)

[12] V. Barashenkov and Y. Smirnov, Existence and stability chart for the ac-driven, damped nonlinear Schrödinger solitons, *Physical Review E*

[13] N. Akhmediev and M. Karlsson , Cherenkov radiation emitted by solitons in optical fibers, *Physical Review A*

[14] J. Mbé, C. Milián and Y. Chembo, Existence and switching behavior of bright and dark Kerr solitons in whispering-gallery mode resonators with zero group-velocity dispersion, *The European Physical Journal D*

[15] C. Milián and D. Skryabin, Soliton families and resonant radiation in a micro-ring resonator near zero group-velocity dispersion,*Optics Express*

[16] P. Parra-Rivas, D. Gomila, F. Leo, S. Coen and L. Gelens, Third-order chromatic dispersion stabilizes Kerr frequency combs, *Optics Letters*

[17] C. Milián, A. Gorbach, M. Taki, A. Yulin and D. Skryabin, Solitons and frequency combs in silica microring resonators: Interplay of the Raman and higher-order dispersion effects, *Physical Review A*

[18] P. Parras-Rivas, D. Gomila, E. Knobloch, S. Coen and L. Gelen, Origin and stability of dark pulse Kerr combs in normal dispersion resonators, *Optics Letters*

[19] V. Lobanov, G. Lihachev, T. Kippenberg and M. Gorodetsky, Frequency combs and platicons in optical microresonators with normal GVD, *Optics Express*

[20] M. Li, M. Zhang, J. Wang, W. Chang, F. Zhou and L. Deng, Flexible Tuning Optical Frequency Combs via Parametric Seeding in Microresonators With Normal Dispersion, *IEEE Photonics Journal*